

# Preparation and Corrosion Resistance of ZIF-8-(5, 6-dimethylbenzimidazole)/LDHs Composite Film on Magnesium Alloy

Huimin Yang<sup>1,2</sup>, Xin Liu<sup>1,2</sup>, Jihui Wang<sup>1,2,\*</sup> and Wenbin Hu<sup>2</sup>

<sup>1</sup> State Key Laboratory of Hydraulic Engineering Simulation and Safety, Tianjin University, Tianjin 300072, P R China;

<sup>2</sup> Tianjin Key Laboratory of Composite and Functional Materials, School of Materials Science and Engineering, Tianjin University, Tianjin 300072, P R China;

\*E-mail: [jhwang@tju.edu.cn](mailto:jhwang@tju.edu.cn)

Received: 22 August 2020 / Accepted: 15 October 2020 / Published: 31 October 2020

---

The following study is conducted to improve the corrosion resistance of magnesium alloy. First, ZnAl layered double hydroxide (ZnAl LDH) film was prepared on AZ61 magnesium alloy by using hydrothermal method. Then, as-prepared ZnAl LDH was put into 2-methylimidazole (2-mIm) solution to synthesize ZIF-8 film (ZIF-8/LDH). Finally, ZIF-8/LDH film synthesized ZIF-8-DMBIM film (ZIF-8-DMBIM/LDHs) via a shell-ligand-exchange-reaction in the methanol solution containing 5, 6-dimethylbenzimidazole (DMBIM). The surface morphology, structure, and composition of the composite film were observed and determined by scanning electronic microscopy, X-ray diffraction, Fourier transform infrared spectroscopy, and energy-dispersive X-ray spectroscopy. The wettability of composite film was measured by using a water contact angle meter, and the corrosion resistance of the composite film was estimated by the polarization curve and electrochemical impedance spectroscopy techniques. Results show that the prepared ZIF-8-DMBIM/LDH composite film has a dense hexagonal plate morphology with a two-layer structure and a thickness of 3.5  $\mu\text{m}$ . Compared with ZnAl LDH and ZIF-8/LDH films, ZIF-8-DMBIM/LDH composite film has a high contact angle ( $115.7^\circ$ ), low corrosion current density, and high corrosion potential and polarization resistance due to its near-smooth surface, dense two-layer structure, and hydrophobic characters.

---

**Keywords:** Magnesium alloy; Corrosion resistance; Composite film; Metal organic framework; Layered double hydroxide; Hydrophobicity

## 1. INTRODUCTION

Magnesium alloys have been widely applied in many industries, such as automotive, aerospace, electronics, and medical equipment, due to their advantages of high strength and low specific gravity [1, 2]. However, the frequent occurrence of serious corrosion problems of magnesium alloys is due to their

high reactivity and porous oxide/hydroxide layer formed by on magnesium alloys, thus considerably limiting their application[3]. Many methods, such as the adjustment of microstructure and composition[4], surface modification[5], surface coating[6], and mixed treatments [7], have been proposed to improve the corrosion resistance of magnesium alloys. Compared with other surface treatments, surface films and coatings on magnesium alloys have elicited extensive attention because of their low cost and simple preparation process.

Layered double hydroxides (LDHs), which are brucite-like lamellar anionic clays with the general formula of  $[M^{2+}_{1-x}M^{3+}_x(OH)_2]^{x+} (A^{n-})_{x/n} \times mH_2O$  ( $M^{2+}$  and  $M^{3+}$  are the divalent and trivalent lamellar metal cations, respectively, and  $A^{n-}$  is the interlayer anion), are mainly employed in many aspects, such as catalysis, adsorption, and drug delivery system, due to their adjustability of host lamellar metal ions, exchangeability of interlayer anions, strong adsorption performance, and thermal stability[8, 9]. LDH films could also be applied as a protection film on magnesium alloys [10]. For example, Zhang [11] fabricated LDH film on magnesium alloy by using the spin coating technique, which effectively inhibited the corrosion of the underlying magnesium alloy. A dense Mg-Al LDH film was successfully prepared on AZ31 alloys by in situ growth method and demonstrated a good protection effect to magnesium alloy [12]. ZnAl LDH layer was first synthesized on magnesium alloys and then modified by stearic acid. The experimental results showed that the as-prepared LDH film had a high corrosion resistance and a superhydrophobic character [13].

Metal–organic frameworks (MOFs), a new type of film candidate, are hybrid porous crystalline materials comprising a metal ion and an organic ligand by a coordination bond. Considering the simplistic preparation, adjustable pore metrics, and easy functionalization of internal surfaces, various MOF materials with demanding specific size, shape, and composition for gas storage[14, 15], separation of small molecules[16, 17], heterogeneous catalysis[18, 19], and drug delivery[20], have been synthesized during the past two decades. The anti-corrosion behavior of MOF composites has recently received increasing attention. MOF/graphite oxide (GO) hybrid materials were fabricated and then added in the epoxy coatings to enhance the anti-corrosion properties of carbon steel[21]. Meanwhile, ZIF-8 (zeolitic imidazolate framework-8), as the flagship of MOF with the chemical formula of  $C_8H_{12}N_4Zn$  (2-methylimidazolate zinc salt), was also widely applied to improve the corrosion resistance of organic coatings due to its ultra-microporous character (with pore limiting diameter of 0.34 nm) and exceptional thermal and chemical stability. For example, GO@ZIF-8[22] and salicylaldehyde@ZIF-8/GO (SZG) [23] composites were respectively fabricated and added in the epoxy and PVB coatings. EIS results proved that these ZIF-8 containing coatings had excellent corrosion protection for mild steel and AA2024 aluminum alloy. However, reports on the in-situ preparation of ZIF-8 coating on magnesium alloys are limited[24, 25].

ZIF-8-DMBIM/LDH composite film was synthesized on AZ61 magnesium alloy by using hydrothermal and ligand exchange reaction methods. The surface and cross-section morphologies, composition, structure, and wettability of composite films were observed and determined by scanning electron microscopy, X-ray diffraction, Fourier transform infrared spectroscopy, energy-dispersive X-ray spectroscopy, contact angle meter, and the corrosion behavior of composite films were investigated by polarization curve and electrochemical impedance spectroscopy (EIS). The protection mechanism of ZIF-8-DMBIM/LDH composite film was proposed and discussed on the basis of the experimental results.

## 2. EXPERIMENTAL

### 2.1. Materials

AZ61 magnesium alloy used with the composition 5.92% Al, 0.49% Zn, 0.15% Mn, of about, 0.037% Si, 0.007% Fe were cut into samples with dimensions of  $10 \times 10 \times 3$  mm. Before the preparation of surface films, AZ61 alloy substrate was mechanically grinded with SiC papers up to 2000 grit, rinsed with deionized water, degreased by acetone and then dried with cold wind for use.  $\text{Zn}(\text{NO}_3)_2 \cdot 6\text{H}_2\text{O}$ ,  $\text{Al}(\text{NO}_3)_3 \cdot 9\text{H}_2\text{O}$ , 2-methylimidazole (2-mIm), 5, 6-dimethylbenzimidazole (DMBIM), triethylamine (TEA) and NaOH were bought from Shanghai Aladdin Industrial Corporation. Methanol and Acetone were purchased from Tianjin Kernel Chemical Company. All the chemical reagents used were in analytical grade.

### 2.2. Preparation of ZnAl LDHs film

ZnAl LDHs film was prepared on AZ61 magnesium alloy by hydrothermal method. 2.97g  $\text{Zn}(\text{NO}_3)_2 \cdot 6\text{H}_2\text{O}$  and 0.39g  $\text{Al}(\text{NO}_3)_3 \cdot 9\text{H}_2\text{O}$  were firstly dissolved in deionized water at room temperature to form a homogeneous solution with the pH value of 10.0 which adjusted by adding 2 mol/L NaOH solution. And then the pretreated AZ61 substrate was put into the obtained solution, transferred to a Teflon-lined stainless-steel container and placed in an oven at 120 °C for 12 h. After reaction, the resultant magnesium alloy was washed with deionized water and dried at room temperature, and then ZnAl- $\text{NO}_3$  LDHs film was formed on magnesium alloy.

### 2.3. Preparation of ZIF-8/LDHs and ZIF-8-DMBIM/LDHs composite film

ZIF-8/LDHs film was synthesized on magnesium alloy as following process. Firstly, 1.00g 2-mIm was added in 50mL methanol to prepare the precursor solution, and then AZ61 substrate with ZnAl- $\text{NO}_3$  LDH film was vertically placed in the above precursor solution and transferred to Teflon-lined stainless-steel vessel. After heated in the oven at 140 °C for 24 h, the vessel was taken out and cooled to room temperature. The acquired samples were then washed with deionized water and dried in air, finally ZIF-8/LDHs composite film was prepared on magnesium alloy. The above-synthesized ZIF-8/LDHs composite film was then immersed in 50 mL methanol solution containing TEA (0.97mL) and DMBIM (1.46g), and transferred to a stainless-steel reactor. After reaction in the oven at 60 °C for 15 h, ZIF-8-DMBIM/LDHs composite film was obtained by washing with methanol and drying at 60 °C.

### 2.4. Characterization

The surface morphology, cross section morphology and composition of composite film were observed and determined by Hitachi S-4800 field emission scanning electron microscopy (FESEM) equipped with an energy dispersive X-ray (EDX) spectroscopy detector. The crystal structure of composite film was measured by X-ray Diffractometer (Rigaku D/MAX 2500×) at a scan speed of

5° min—1 in the 2θ range of 5–70° with Cu Kα radiation (40 kV, 40 mA, λ = 0.154 nm). FTIR spectrum of composite film was investigated by using FTIR-850 spectrophotometer in the 4000–400 cm<sup>-1</sup> region via KBr tablet method.

The static contact angle of composite film was determined by using JC2000D optical contact angle meter at ambient temperature with the water drop volume of 7 μL. The value of contact angle was obtained by the average of five measurements on different positions of film surface.

### 2.5. Corrosion resistance

The corrosion behavior of AZ61 substrate with and without composite film was measured in 3.5% NaCl solution at room temperature by using polarization curve and electrochemical impedance spectroscopy (EIS) techniques on Autolab 302 electrochemical workstation. Before measurement, when the sample is immersed in a 3.5% NaCl solution for 0.5-1 h to reach stable open circuit potential. A three-electrode system was applied with AZ61 substrate with and without composite film as work electrode (1cm<sup>2</sup>), and a platinum plate and saturated calomel electrode (SCE) were applied as the counter electrode and reference electrode respectively.

The polarization curves of samples were measured from -0.5V to 0.5V versus open circuit potential (OCP) at the scan rate of 1.667 mV/s. And then the protection efficiency of composite film was calculated by the following equations:

$$\eta_1 = \frac{i_{\text{corr}} - i'_{\text{corr}}}{i_{\text{corr}}} \times 100\% \quad 1)$$

Where  $\eta_1$  is the protection efficiency by polarization curve;  $i_{\text{corr}}$  is the corrosion current density of AZ61 substrate in 3.5% NaCl solution.  $i'_{\text{corr}}$  is the corrosion current density of AZ61 substrate with composite film in 3.5% NaCl solution.

EIS measurements of AZ61 substrate with and without composite film were conducted under the open circuit potential (OCP) with the AC voltage amplitude of 10mV in the frequency range of 10<sup>5</sup> Hz to 10<sup>-2</sup> Hz. After measurements, ZsimpWin software was applied to analyze the obtained EIS spectrum. The protection efficiency of composite film was calculated by the following equation:

$$\eta_2 = \frac{R'_{\text{total}} - R_{\text{total}}}{R'_{\text{total}}} \times 100\% \quad 2)$$

Where  $R_{\text{total}}$  is the polarization resistance of AZ61 substrate in 3.5% NaCl solution, and  $R'_{\text{total}}$  is the total polarization resistance of AZ61 samples with composite film in 3.5% NaCl solution.

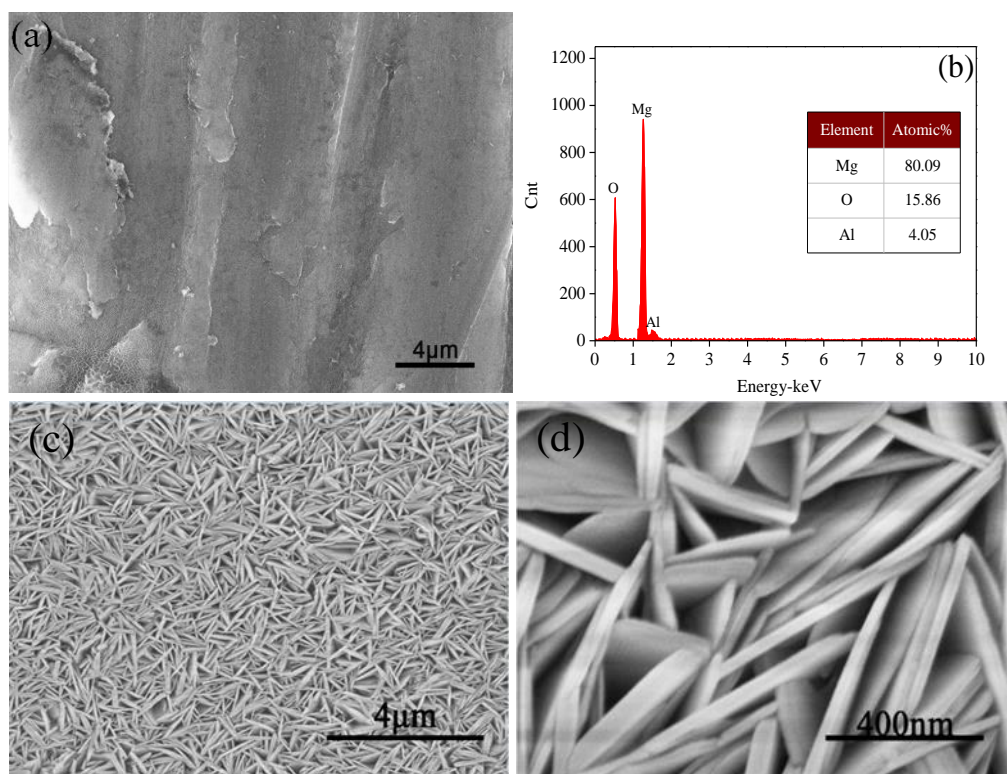
## 3. RESULTS

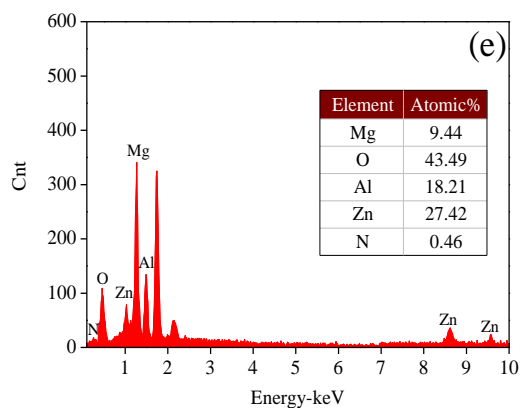
### 3.1. Surface morphology

Figure 1 is the surface morphology and EDS spectrum of AZ61 magnesium alloy and ZnAl-NO<sub>3</sub> LDHs film on AZ61 substrate. It can be seen that AZ61 magnesium alloy is in a rough surface (Figure

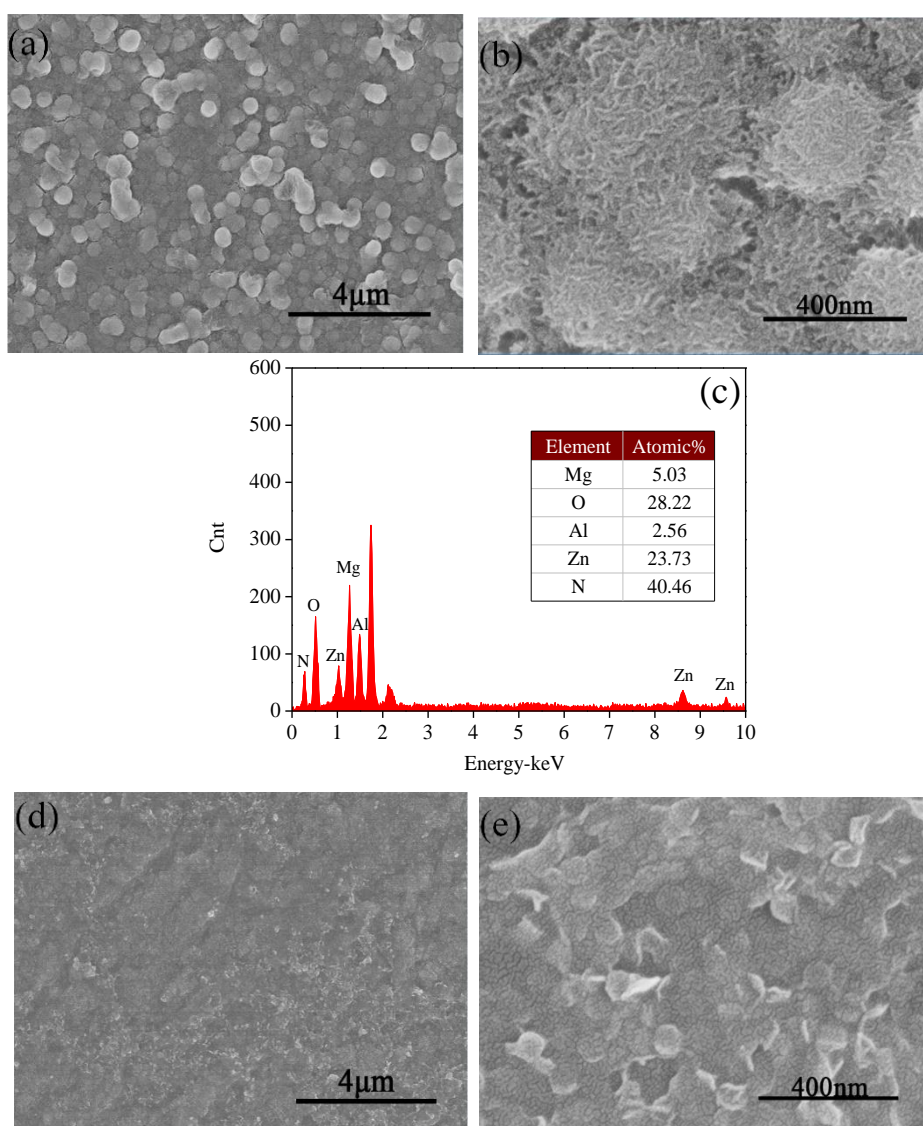
1a) with the composition of Mg, Al and O elements (Figure 1b), which indicating that there is an oxide or hydroxide film on magnesium substrate. After the formation of ZnAl-NO<sub>3</sub> LDHs film, AZ61 alloy is in a lamellar structure with a thickness of 40nm which vertically grown on the substrate (Figure 1c and 1d). In the EDS spectrum of ZnAl-NO<sub>3</sub> LDHs film (Figure 1e), the content of Mg element is reduced from 80.09% to 9.44% whereas the content of Al and O elements is increased from 4.05% and 15.86% to 18.21% and 43.49% respectively. Meanwhile Zn and N elements are appeared in the ZnAl-NO<sub>3</sub> LDHs film. All these results show that ZnAl-NO<sub>3</sub> LDHs LDHs film was successfully formed on AZ61 substrate.

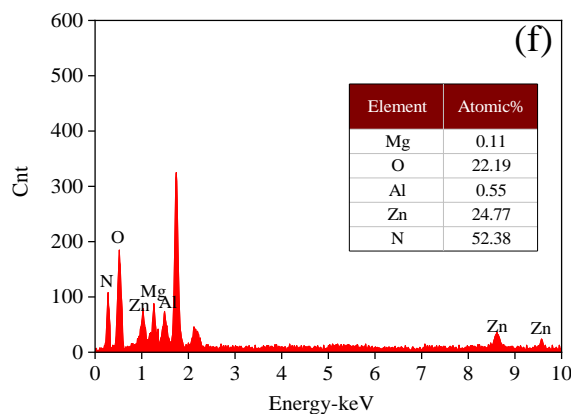
The surface morphology and EDS spectrum of ZIF-8/LDHs and ZIF-8-DMBIM/LDHs composite film are shown in Figure 2. It can be observed that ZIF-8/LDHs composite film is in a hexagonal plate morphology with microporous structures (Figure 2a and 2b). The content of Al and O elements in ZIF-8/LDHs composite film is less than that of ZnAl-NO<sub>3</sub> LDHs film, whereas the content of N element is increased to 40.46% which is higher than that in ZnAl-NO<sub>3</sub> LDHs film (Figure 2c). These results indicate that ZIF-8 film was assembled on the ZnAl-NO<sub>3</sub> LDHs film. Compared with ZIF-8/LDHs film, ZIF-8-DMBIM/LDHs composite film has a near-smooth and dense hexagonal plate morphology (Figure 2d and 2e). The content of Mg, Al and O elements in ZIF-8-DMBIM/LDHs is a little bit less than that of ZIF-8/LDHs composite film, whereas the content of Zn and N elements is slightly larger than that of ZIF-8/LDHs composite film (Figure 2f), which is probably caused by the less influence of AZ61 substrate and ZnAl-NO<sub>3</sub> LDHs film.





**Figure 1.** Surface morphology and EDS spectrum of AZ61 substrate (a, b) and ZnAl-NO<sub>3</sub> LDHs film (c, d, e).

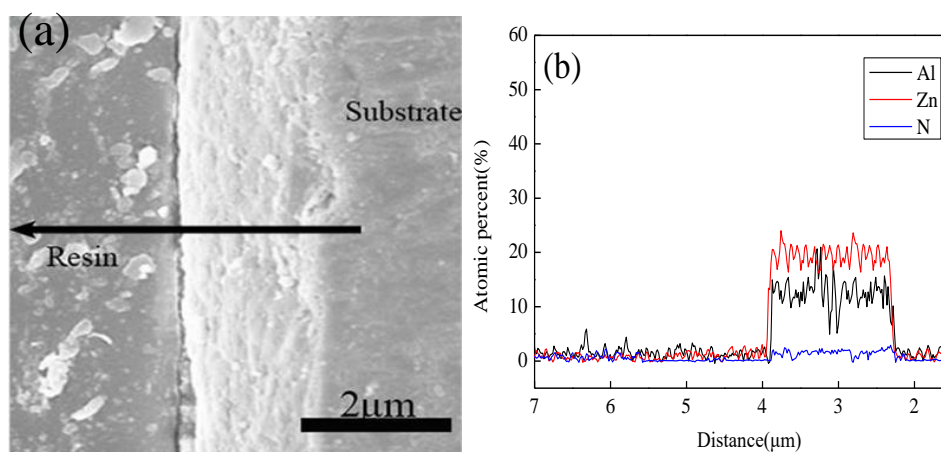


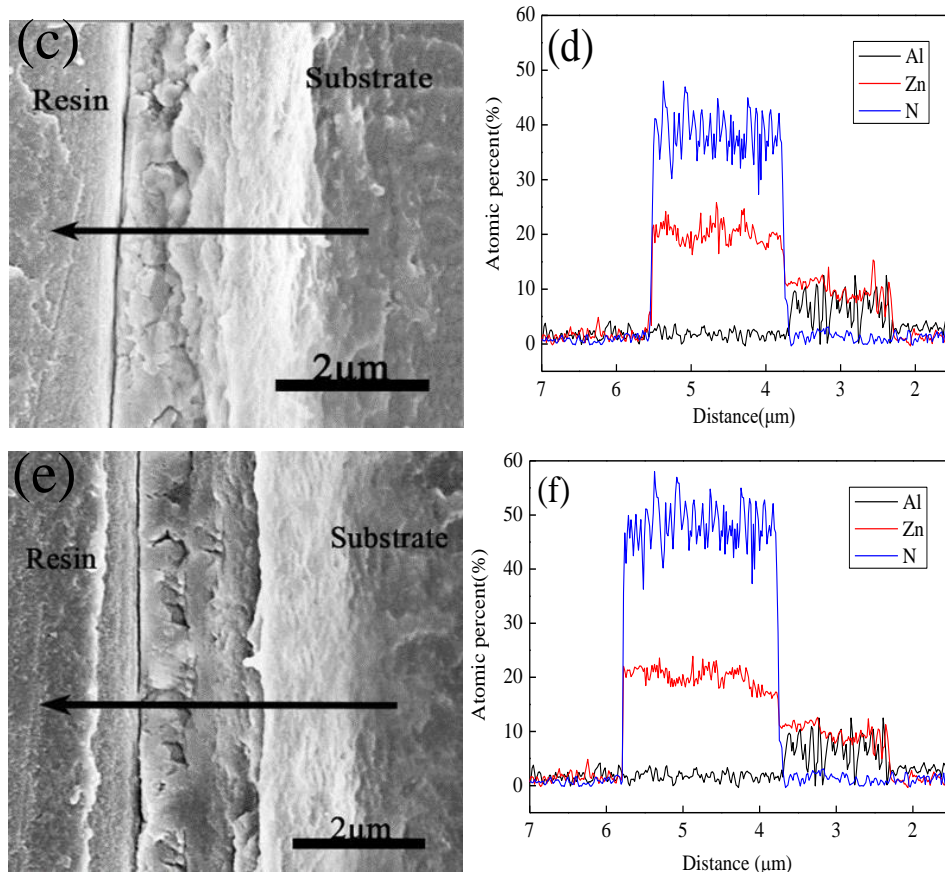


**Figure 2.** Surface morphology and EDS spectrum of ZIF-8/LDHs (a, b, c) and ZIF-8-DMBIM/LDHs film (d, e, f).

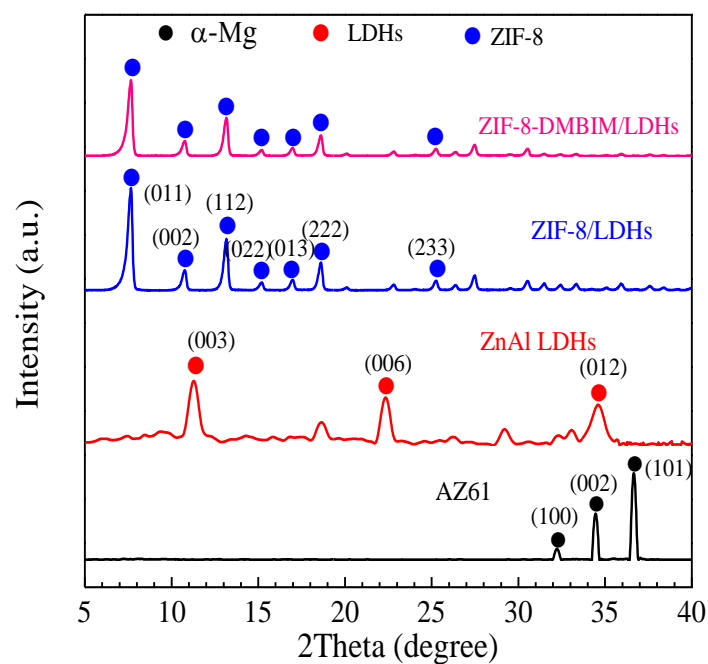
### 3.2. Cross section morphology

Figure 3 is the cross-sectional morphology and elements distribution of ZnAl-NO<sub>3</sub> LDHs, ZIF-8/LDHs and ZIF-8-DMBIM/LDHs film. It can be seen that ZnAl-NO<sub>3</sub> LDHs film with the thickness of 1.7 μm and composition of Zn, Al and N elements is closely located on AZ61 substrate (Figure 3a and 3b). After the formation of ZIF-8 film on ZnAl-NO<sub>3</sub> LDHs, ZIF-8/LDHs composite film is in a double layer structure, in which the inner layer is ZnAl-NO<sub>3</sub> LDHs and the outer layer is the newly formed ZIF-8 film (Figure 3c). The inner ZnAl-NO<sub>3</sub> LDHs film in ZIF-8/LDHs has almost the same composition as single ZnAl-NO<sub>3</sub> LDHs film but with a lower thickness (1.2 μm) than that of single ZnAl-NO<sub>3</sub> LDHs film, and the outer ZIF-8 film with the thickness of 1.7 μm has a higher Zn and N content but a lower Al content when compared with ZnAl-NO<sub>3</sub> LDHs film (Figure 3d), which indicating that ZIF-8 film is formed by the reaction between 2-mIm in the solution and parts of ZnAl-NO<sub>3</sub> LDHs film. After the exchange reaction in DMBIM solution, ZIF-8-DMBIM/LDHs film is also in a double layer structure (Figure 3e), in which the inner layer is ZnAl-NO<sub>3</sub> LDHs with the same composition and thickness as that in ZIF-8/LDHs composite film and the outer layer has the higher N content and larger thickness (2.0 μm) than that in ZIF-8/LDHs composite film (Figure 3f). These results mean that the exchange reaction is occurred between DMBIM in the solution and 2-mIm on the top ZIF-8 layer, and thus the thickness of outer layer is increased form 1.7 μm to 2.0 μm.





**Figure 3.** Cross section morphology and elements distribution of ZnAl-NO<sub>3</sub> LDHs film (a, b), ZIF-8/LDHs film (c, d) and ZIF-8-DMBIM/LDHs film (e, f).



**Figure 4.** XRD pattern of AZ61 substrate, ZnAl-NO<sub>3</sub> LDHs, ZIF-8/LDHs and ZIF-8-DMBIM/LDHs film.

### 3.3. Structure

Figure 4 is the XRD pattern of AZ61 substrate, ZnAl-NO<sub>3</sub> LDHs, ZIF-8/LDHs and ZIF-8-DMBIM/LDHs film. In the spectrum of AZ61 substrate, the diffraction peaks are appeared at 32.2°, 34.4° and 36.6°, which corresponding to (100), (002), and (101) crystal planes of  $\alpha$ -Mg phase in magnesium alloy [26]. After the formation of ZnAl-NO<sub>3</sub> LDHs film, there are three diffraction peaks at 11.7°, 23.5° and 34.6° existed in the pattern, which are indexed to (003), (006) and (012) planes of ZnAl LDHs phase [27]. By calculation, the basal spacing of (003) plane is 0.799 nm, which means that ZnAl-NO<sub>3</sub> LDHs film has been successfully prepared on AZ61 substrate [27]. In the XRD pattern of ZIF-8/LDHs, the diffraction peaks at 7.3°, 10.3°, 12.7°, 14.7°, 16.6°, 18.2° and 24.6° are observed, which are corresponded to (011), (002), (112), (022), (013), (222) and (233) planes of crystalline ZIF-8 phase [28]. After the exchange reaction in DMBIM solution, the diffraction peaks of ZIF-8-DMBIM/LDHs film are the same as that of ZIF-8/LDHs film, which means that the exchange reaction is mainly occurred in the outermost layer of ZIF-8 crystals and thus the obtained ZIF-8-DMBIM film has the original ZIF-8 crystal structure [29].

The FTIR spectrum of ZnAl-NO<sub>3</sub> LDHs, ZIF-8/LDHs and ZIF-8-DMBIM/LDHs film is shown in Figure 5. For ZnAl-NO<sub>3</sub> LDHs, the broad absorption peaks at 3436 cm<sup>-1</sup> and 3702 cm<sup>-1</sup> are attributed to the stretching vibration of hydroxyl groups of LDH layer and LDH interlayer water molecules [30]. And the absorption peak at 1384 cm<sup>-1</sup> is belonged to the stretching vibration of NO<sub>3</sub><sup>-</sup>, which indicating the formation of LDH intercalated with NO<sub>3</sub><sup>-</sup> on AZ61 substrate [31]. In the FTIR spectrum of ZIF-8/LDHs, the peak at 3693 cm<sup>-1</sup> is ascribed to the stretching vibration of hydroxyl groups and interlayer water of LDHs. The absorption peaks at 3134 cm<sup>-1</sup> and 2928 cm<sup>-1</sup> are attributed to the aromatic C-H stretching and aliphatic C-H stretch of imidazole, and the absorption peaks at 1147 cm<sup>-1</sup> and 1434 cm<sup>-1</sup> are associated with the absorption of C-N bonds and specific vibration transitions imidazole ring respectively [32, 33]. Meanwhile, the peak appearing at 422 cm<sup>-1</sup> is designated to the stretching vibration of Zn-N [34]. All these results demonstrate that ZIF-8 film is successfully synthesized on magnesium alloy. In the spectrum of the ZIF-8-DMBIM/LDHs film, apart from the above absorption peaks of ZIF-8/LDHs, two absorption peaks at 805 cm<sup>-1</sup> and 854 cm<sup>-1</sup> are observed, which are designated to the C-H out-of-plane deformation vibrations in the phenyl rings of DMBIM [29]. These two absorption peaks prove that the exchange reaction between DMBIM and 2-mIm is actually occurred during the formation of ZIF-8-DMBIM/LDHs composite film.

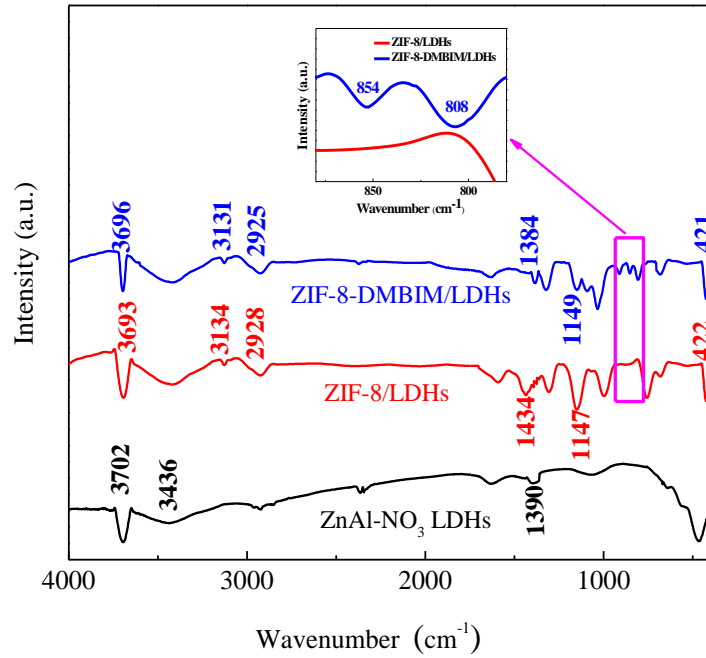


**Figure 5.** FTIR spectrum of ZnAl-NO<sub>3</sub> LDHs, ZIF-8/LDHs and ZIF-8-DMBIM/LDHs film.

### 3.4. Surface wettability

Figure 6 is the water drop morphology on AZ61 substrate, ZnAl-NO<sub>3</sub> LDHs, ZIF-8/LDHs and ZIF-8-DMBIM/LDHs film during the static contact angle measurement. By calculation, the static contact angle of AZ61 substrate, ZnAl-NO<sub>3</sub> LDHs, ZIF-8/LDHs and ZIF-8-DMBIM/LDHs film are 7.7° (Figure 4a), 14.4° (Figure 4b), 45.0° (Figure 4c) and 115.7° (Figure 4d) respectively, which infers that AZ61 substrate, ZnAl-NO<sub>3</sub> LDHs, ZIF-8/LDHs film are in a hydrophilic state whereas ZIF-8-DMBIM/LDHs film is in a hydrophobic state.

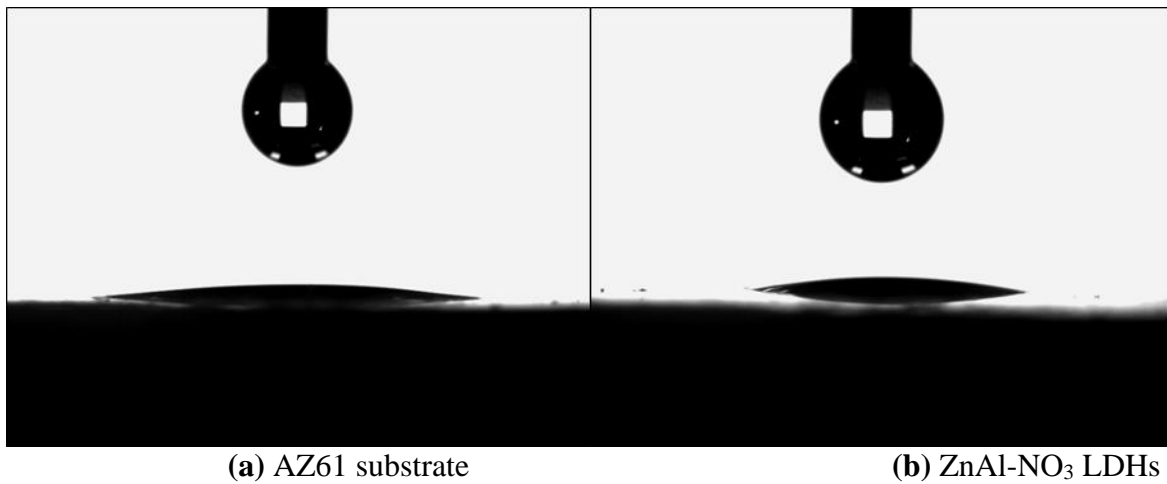




**Figure 6.** Water drop morphology on AZ61 substrate, ZnAl-NO<sub>3</sub> LDHs, ZIF-8/LDHs and ZIF-8-DMBIM/LDHs film during the static contact angle measurement.

### 3.5. Polarization curve

The polarization curve of AZ61 substrate, ZnAl-NO<sub>3</sub> LDHs, ZIF-8/LDHs and ZIF-8-DMBIM/LDHs film in a 3.5% NaCl solution is shown in Figure 7, and the corrosion potential ( $E_{\text{corr}}$ ), current density ( $I_{\text{corr}}$ ) and protection efficiency ( $\eta_1$ ) were calculated and listed in Table 1. In 3.5% NaCl solution, AZ61 magnesium alloy has a lower corrosion potential of -1.556V and a higher corrosion density of 39.903  $\mu\text{A}/\text{cm}^2$ . After the formation of ZnAl-NO<sub>3</sub> LDHs, ZIF-8/LDHs and ZIF-8-DMBIM/LDHs film on AZ61 substrate, the corrosion potential of films is increased positively to -1.431V, -0.596V and -0.165V respectively, and the corrosion current density of films is decreased to 26.363  $\mu\text{A}/\text{cm}^2$ , 7.047  $\mu\text{A}/\text{cm}^2$  and 2.399  $\mu\text{A}/\text{cm}^2$ . So, the protection efficiency of ZnAl-NO<sub>3</sub> LDHs, ZIF-8/LDHs and ZIF-8-DMBIM/LDHs film to AZ61 substrate is improved from 33.93%, 82.34% to 93.99%, which indicating that the prepared composite film especially the ZIF-8-DMBIM/LDHs film has a better protection effect to AZ61 magnesium alloy.

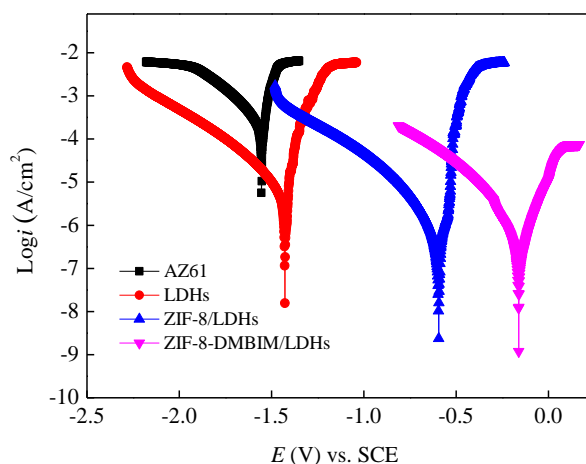


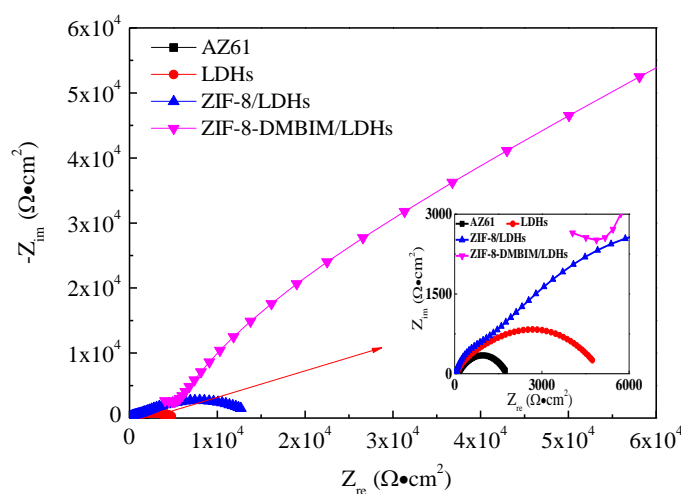
**Figure 7.** Polarization curves of AZ61 substrate, ZnAl-NO<sub>3</sub> LDHs, ZIF-8/LDHs and ZIF-8-DMBIM/LDHs film in 3.5% NaCl solution.

**Table 1.**  $E_{corr}$ ,  $I_{corr}$  and  $\eta_1$  of AZ61 substrate, ZnAl-NO<sub>3</sub> LDHs, ZIF-8/LDHs and ZIF-8-DMBIM/LDHs film in 3.5% NaCl solution.

| Simple                         | AZ61   | ZnAl-NO <sub>3</sub> LDHs | ZIF-8/LDHs | ZIF-8-DMBIM/LDHs |
|--------------------------------|--------|---------------------------|------------|------------------|
| $E_{corr}/V_{SCE}$             | -1.556 | -1.431                    | -0.596     | -0.165           |
| $I_{corr}/\mu A \cdot cm^{-2}$ | 39.90  | 26.36                     | 7.05       | 2.40             |
| $\eta_1/\%$                    | ----   | 33.93                     | 82.34      | 93.99            |

3.6. EIS spectrum

Figure 8 is the EIS spectrum of AZ61 substrate, ZnAl-NO<sub>3</sub> LDHs, ZIF-8/LDHs and ZIF-8-DMBIM/LDHs film in 3.5% NaCl solution. It can be found from Figure 8 that in the EIS spectrum of AZ61 substrate there is only one capacitive arc with the impedance modulus at 0.01 Hz of  $1.70 \times 10^3 \Omega \cdot cm^2$ . After the formation of ZnAl-NO<sub>3</sub> LDHs film on AZ61 substrate, there are two capacitive arcs founded with the impedance modulus of  $4.70 \times 10^3 \Omega \cdot cm^2$ , which is larger than that of AZ61 substrate. In these two capacitive arcs, the capacitive arc at higher frequency is coming from the capacitance  $Q_{LDHs}$  and resistance  $R_{LDHs}$  of ZnAl-NO<sub>3</sub> LDHs film, whereas the capacitive arc at low frequency is resulting from the double layer capacitance  $Q_{dl}$  and charge transfer resistance  $R_{ct}$  of AZ61 substrate. As the formation of ZIF-8 and ZIF-8-DMBIM on ZnAl-NO<sub>3</sub> LDHs film, there are three capacitive arcs existed with the impedance modulus at 0.01 Hz of  $2.6 \times 10^5 \Omega \cdot cm^2$  and  $1.1 \times 10^6 \Omega \cdot cm^2$ , which are originated from the capacitance  $Q_{Z/L}$  and resistance  $R_{Z/L}$  of ZIF-8 film or ZIF-8-DMBIM film, capacitance  $Q_{LDHs}$  and resistance  $R_{LDHs}$  of ZnAl-NO<sub>3</sub> LDHs film and double layer capacitance  $Q_{dl}$  and charge transfer resistance  $R_{ct}$  of AZ61 substrate respectively. These results proved that ZIF-8/LDHs and ZIF-8-DMBIM/LDHs composite film are in double layer structure and the corrosion resistance of AZ61 substrate is greatly improved by the composite film.



(a) Nyquist plot

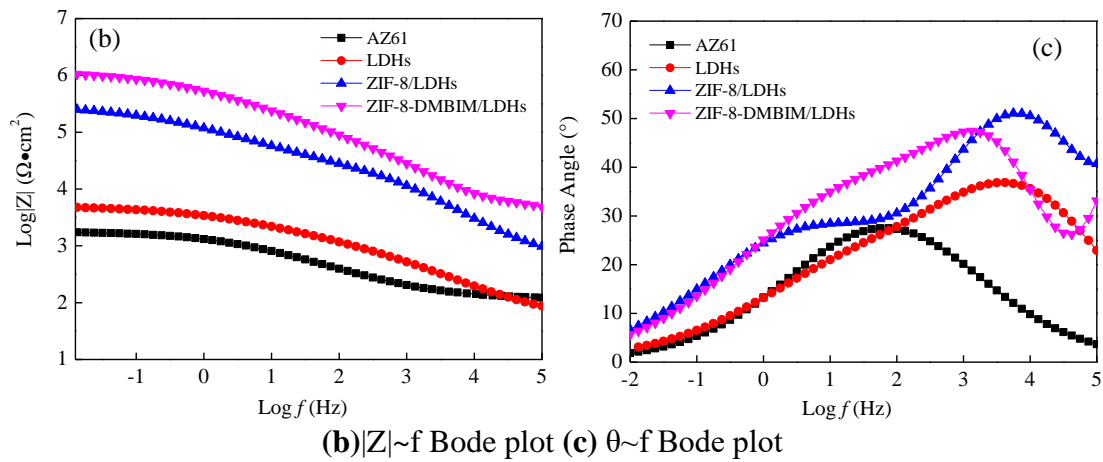


**Figure 8.** EIS spectrum of AZ61 substrate, ZnAl-NO<sub>3</sub> LDHs, ZIF-8/LDHs and ZIF-8-DMBIM/LDHs film in 3.5% NaCl solution in 3.5% NaCl solution.

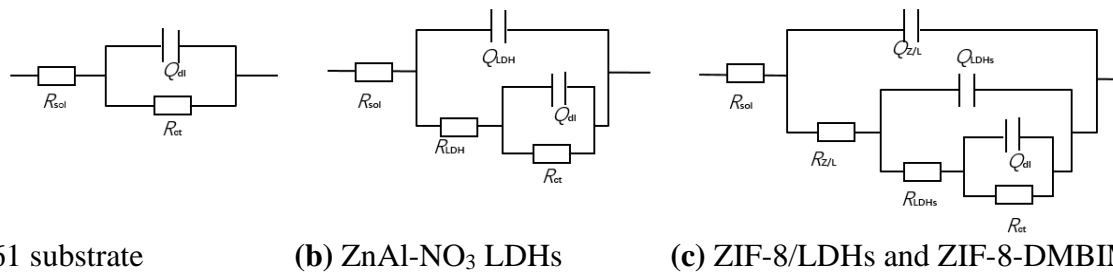


**Figure 9.** Equivalent circuits applied for AZ61 substrate, ZnAl-NO<sub>3</sub> LDHs, ZIF-8/LDHs and ZIF-8-DMBIM/LDHs film in 3.5% NaCl solution.

By the above consideration, the equivalent circuits in Figure 9 were used to fit the obtained EIS data, and the corresponding electrochemical parameters are listed in Table 2. In the equivalent circuits,  $R_{sol}$  represents the solution resistance,  $R_{Z/L}$  and  $Q_{Z/L}$  represent the resistance and capacitance of the ZIF-8 or ZIF-8-DMBIM film respectively,  $R_{LDHs}$  and  $Q_{LDHs}$  are the resistance and capacitance of the ZnAl-NO<sub>3</sub> LDHs film,  $Q_{dl}$  and  $R_{ct}$  represent the double layer capacitance and charge transfer resistance of AZ61 substrate.

**Table 2.** Fitting electrochemical parameters and protection efficiency  $\eta_2$  of AZ61 substrate, ZnAl-NO<sub>3</sub> LDHs, ZIF-8/LDHs and ZIF-8-DMBIM/LDHs film in 3.5% NaCl solution.

| Sample                                      | AZ61  | ZnAl-NO <sub>3</sub> LDHs | ZIF-8/LDHs            | ZIF-8-DMBIM/LDHs      |
|---|-------|---------------------------|-----------------------|-----------------------|
| $R_{sol}/(\Omega \cdot cm^2)$               | 53.80 | 52.69                     | 43.90                 | 45.50                 |
| $Y_0/(\Omega^{-1} \cdot cm^{-2} \cdot s^n)$ | ---   | ---                       | $1.56 \times 10^{-7}$ | $8.12 \times 10^{-9}$ |
| $n_{Z/L}$                                   | ---   | ---                       | 0.89                  | 0.81                  |
| $R_{Z/L}/(\Omega \cdot cm^2)$               | ---   | ---                       | 41.32                 | 5201.00               |

|  |                       |                       |                       |                       |
|--|-----------------------|-----------------------|-----------------------|-----------------------|
| $Q_{LDHs^-}$   | ----                  | $9.18 \times 10^{-6}$ | $1.12 \times 10^{-7}$ | $2.29 \times 10^{-8}$ |
| $Y_0/(\Omega^{-1} \cdot \text{cm}^{-2} \cdot \text{s}^n)$        | ----                  |                       |                       |                       |
| $n_{LDHs}$   | ----                  | 0.81                  | 0.86                  | 0.82                  |
| $R_{LDHs}/(\Omega \cdot \text{cm}^2)$                            | ----                  | $1.08 \times 10^3$    | $1.11 \times 10^3$    | $3.74 \times 10^4$    |
| $Q_{dl-Y_0}/(\Omega^{-1} \cdot \text{cm}^{-2} \cdot \text{s}^n)$ | $1.20 \times 10^{-4}$ | $7.64 \times 10^{-5}$ | $2.89 \times 10^{-6}$ | $5.22 \times 10^{-7}$ |
| $n_{dl}$   | 0.86                  | 0.80                  | 0.83                  | 0.87                  |
| $R_{ct}/(\Omega \cdot \text{cm}^2)$                              | $1.68 \times 10^3$    | $3.98 \times 10^3$    | $1.36 \times 10^4$    | $1.21 \times 10^6$    |
| $R_{total}/(\Omega \cdot \text{cm}^2)$                           | $1.68 \times 10^3$    | $5.06 \times 10^3$    | $1.48 \times 10^4$    | $1.25 \times 10^6$    |
| $\eta_2/\%$  | ----                  | 66.80                 | 88.65                 | 99.87                 |

From Table 2, it can be seen that the polarization resistance of AZ61 substrate in 3.5% NaCl solution is  $1.68 \times 10^3 \Omega \cdot \text{cm}^2$ . After the formation of ZnAl-NO<sub>3</sub> LDHs, ZIF-8/LDHs and ZIF-8-DMBIM/LDHs film on AZ61 substrate, the total polarization resistance is increased gradually from  $5.06 \times 10^3 \Omega \cdot \text{cm}^2$ ,  $1.48 \times 10^4 \Omega \cdot \text{cm}^2$  to  $1.25 \times 10^6 \Omega \cdot \text{cm}^2$ . Meanwhile the protection efficiency of ZnAl-NO<sub>3</sub> LDHs, ZIF-8/LDHs and ZIF-8-DMBIM/LDHs film is enhanced from 66.80%, 88.65% to 99.87%, which is accorded with the protection efficiency by polarization curve in Table 1. It's also noticed that with the successive formation of ZnAl-NO<sub>3</sub> LDHs, ZIF-8/LDHs and ZIF-8-DMBIM/LDHs film on AZ61 substrate, the capacitance  $Q_{ZL}$  is reduced from  $1.56 \times 10^{-7} \mu\text{F} \cdot \text{cm}^{-2}$  of ZIF-8/LDHs film to  $8.12 \times 10^{-9} \mu\text{F} \cdot \text{cm}^{-2}$  of ZIF-8-DMBIM/LDHs film, and the capacitance  $Q_{LDHs}$  is decreased from  $9.18 \times 10^{-6} \mu\text{F} \cdot \text{cm}^{-2}$  (ZnAl-NO<sub>3</sub> LDHs film),  $1.12 \times 10^{-7} \mu\text{F} \cdot \text{cm}^{-2}$  (ZIF-8/LDHs film) to  $2.29 \times 10^{-8} \mu\text{F} \cdot \text{cm}^{-2}$  (ZIF-8-DMBIM/LDHs film). These results suggest that the water absorption resistance is improved by the formation of ZnAl-NO<sub>3</sub> LDHs, ZIF-8/LDHs and ZIF-8-DMBIM/LDHs film[35], and thus the corrosion resistance of magnesium alloy is enhanced gradually

## 4. DISCUSSION

The above experimental results reveal that the prepared ZIF-8-DMBIM/LDH composite film has an excellent protection effect on the underneath AZ61 magnesium alloy. The high corrosion resistance of the composite film is attributed to its near-smooth surface, dense double-layer structure, and hydrophobic characteristic.

### 4.1. Formation of composite film

AZ61 magnesium alloy was first immersed in the solution containing Zn (NO<sub>3</sub>)<sub>2</sub> and Al (NO<sub>3</sub>)<sub>3</sub> to improve the corrosion resistance. ZnAl-NO<sub>3</sub> LDH film with laminar structure was grown vertically on magnesium alloy under the hydrothermal reaction (Figures 1c, 1d, 3a, and 10). This result is remarkably consistent with the relevant literature [36]. Liu [37] proposed that the formation of the ZIF-8 crystal nucleus follows a similar mechanism. Therefore, when the as-obtained ZnAl-NO<sub>3</sub> LDHs film was put in the 2-methylimidazole/methanol solution, zinc ions on the host lamellar plate of ZnAl-NO<sub>3</sub> LDH film were then reacted with 2-methylimidazole in the solution to form the ZIF-8 crystal nucleus. Finally, the ZIF-8 crystal film with hexagonal and microporous morphology was gradually formed on the surface of the ZnAl-NO<sub>3</sub> LDH film (Figures 2a, 2b, and 10). This reaction occurred in the top layer

of the ZnAl-NO<sub>3</sub> LDH film. Thus, the formed ZIF-8/LDH composite film had a double-layer structure: the outer layer comprised ZIF-8 with high contents of Zn and N elements, and the inner layer remained as ZnAl-NO<sub>3</sub> LDHs with a thickness less than that of the original ZnAl-NO<sub>3</sub> LDHs (Figures 3c and 3d), which is consistent with previous reports[37,38].

Considering the modification of as-synthesized composite film, ZIF-8/LDH film was exposed in the 5, 6-dimethylbenzimidazole (DMBIM) methanol solution. After the ligand exchange reaction between DMBIM and 2-mIm, the outermost shell of ZIF-8 film was converted into ZIF-8-DMBIM (Figure 10). Thus, the ZIF-8-DMBIM/LDH composite film was prepared with a near-smooth surface, dense double-layer structure (Figures 2d, 2e, 3e, and 10), and thickness larger than that of ZIF-8/LDH film (Figures 3c, 3e, and 10). The formation process of ZIF-8-DMBIM/LDH composite film on magnesium alloys could be summarized in Figure 10.

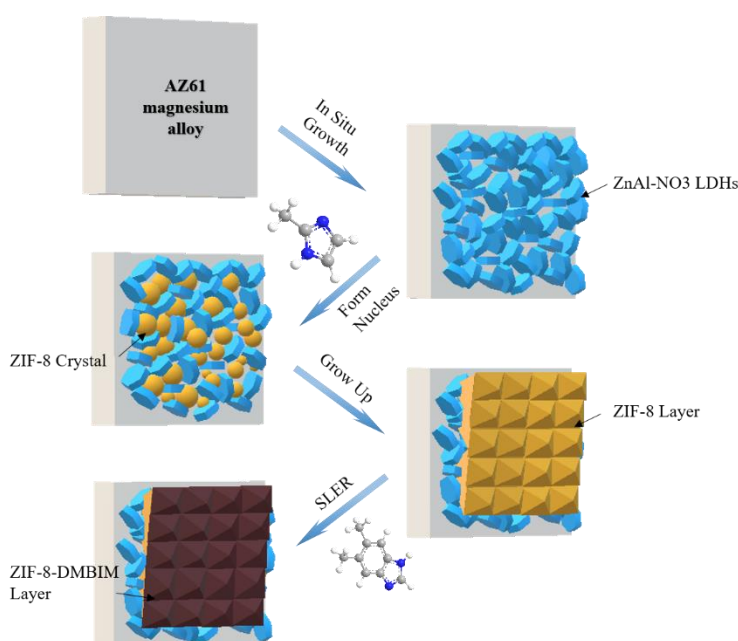


**Figure 10.** Growth mechanism of ZIF-8-DMBIM/LDHs composite film

#### 4.2. Protection mechanism

The surface morphology and the formation process of composite films revealed that ZIF-8-DMBIM/LDH composite film has a near-smooth surface (Figures 2d and 2e) and a hydrophobic characteristic (Figure 6d). Penetration into the composite film by the corrosive ions and water molecules in the solution is difficult when the magnesium alloy is immersed in the corrosive solution, thus effectively protecting the magnesium alloy underneath. Considering the microporous morphology (Figures 2a and 2b) and the hydrophilic characteristic (Figure 6c), which are consistent with the view proposed by Liu [29], ZIF-8/LDH composite film has a lower corrosion resistance than that of ZIF-8-DMBIM/LDH composite film.

The cross-section morphology revealed that ZIF-8-DMBIM/LDH composite film has a double-layer structure (Figures 3e and 3f). Moreover, the EIS spectrum of the composite film in 3.5% NaCl solution has three capacitive arcs (Figure 8) corresponding to the ZIF-8-DMBIM layer, ZnAl-NO<sub>3</sub> LDHs

layer, and AZ61 substrate (Figure 9c). Compared with single ZnAl-NO<sub>3</sub> LDHs film, ZIF-8/LDHs and ZIF-8-DMBIM/LDHs composite films have long diffusion channels of chloride ions and water molecules to the magnesium substrate because of the physical barrier effect of double-layer structures. Meanwhile, penetration to the hydrophobic ZIF-8-DMBIM/LDH composite film by the corrosive ions and water molecules in the solution is difficult to, as proven by the low capacitance of  $Q_{Z/L}$  and  $Q_{LDHs}$  (Table 2) [35]. Therefore, compared with the previous research literature [38,39], the prepared ZIF-8-DMBIM/LDH composite film has a larger corrosion resistance than that of ZIF-8/LDH composite and single ZnAl-NO<sub>3</sub> LDH films (Figures 7 and 8, respectively).

## 5. CONCLUSIONS

1. ZIF-8-DMBIM/LDHs composite film has been successfully synthesized by using hydrothermal method and ligand exchange reaction. The synthesized ZIF-8-DMBIM/LDHs composite film with the thickness of 3.2  $\mu\text{m}$  has a near-smooth surface, dense double layer structure and a hydrophobic characteristic.

2. With the formation of ZnAl-NO<sub>3</sub> LDHs, ZIF-8/LDHs and ZIF-8-DMBIM/LDHs film on AZ61 substrate, the protection efficiency of AZ61 magnesium alloy is increased from 66.80%, 88.65% to 99.87%. Compared with ZnAl-NO<sub>3</sub> LDHs and ZIF-8/LDHs films, ZIF-8-DMBIM/LDHs composite film has a higher contact angle (115.7°), higher corrosion potential and polarization resistance due to its near-smooth surface, dense double layer structure and hydrophobic characteristic.

In summary, with the ligand exchange reaction concept, for the first time we have successfully prepared anticorrosive ZIF-8-DMBIM/LDHs composite film on Mg alloy. Taking into consideration the fact that hydrophobic MOFs from predesigned organic ligands can also be prepared. It is believed that the stabilized MOF materials are expected to be suitable for anticorrosion applications under different corrosive environment.

## FUNDING

This work was supported by National Natural Science Foundation of China (No. 51771133 and 51471117) and National Basic Research Program of China (2014CB046801).

## References

1. M. Zhou, L. Yan, H. Ling, Y. Diao, X. Pang, Y. Wang and K. Gao, *Appl. Surf. Sci.*, 404 (2017) 246.
2. F. Witte, *Acta Biomater.*, 6 (2010) 1680.
3. G. Zhang, A. Tang, L. Wu, Z. Zhang, H. Liao, Y. Long, L. Li, A. Atrens and F. Pan, *Surf. Coat. Technol.*, 366 (2019) 238.
4. D. Song, A. B. Ma, J. H. Jiang, P. H. Lin, D. H. Yang and J. F. Fan, *Corros. Sci.*, 53 (2011) 362.
5. M. He, L. Liu, Y. Wu, Z. Tang and W. Hu, *J. Coat. Technol. Res.*, 6 (2009) 407.
6. M.-a. Chen, N. Cheng, Y.-c. Ou and J.-m. Li, *Surf. Coat. Technol.*, 232 (2013) 726.
7. X.-J. Cui, M.-T. Li, R.-S. Yang and Z.-X. Yu, *Appl. Surf. Sci.*, 363 (2016) 91.
8. G. R. Williams and D. O'Hare, *J. Mater. Chem.*, 16 (2006) 3065.
9. S. Tang, Y. Yao, T. Chen, D. Kong, W. Shen and H. K. Lee, *Anal. Chim. Acta*, 1103 (2020) 32.
10. F. Wu, J. Liang, Z. Peng and B. Liu, *Appl. Surf. Sci.*, 313 (2014) 834.
11. F. Zhang, M. Sun, S. Xu, L. Zhao and B. Zhang, *Chem. Eng. J.*, 141 (2008) 362.

12. J. Chen, Y. Song, D. Shan and E.-H. Han, *Corros. Sci.*, 53 (2011) 3281.
13. M. Zhou, X. Pang, L. Wei and K. Gao, *Appl. Surf. Sci.*, 337 (2015) 172.
14. O. K. Farha, A. O. Yazaydin, I. Eryazici, C. D. Malliakas, B. G. Hauser, M. G. Kanatzidis, S. T. Nguyen, R. Q. Snurr and J. T. Hupp, *Nat. Chem.*, 2 (2010) 944.
15. S. Ma and H.-C. Zhou, *Chem. Commun.*, 46 (2010) 44.
16. B. Chen, Y. Yang, F. Zapata, G. Lin, G. Qian and E. B. Lobkovsky, *Adv. Mater.*, 19 (2007) 1693.
17. B. Chen, S. Xiang and G. Qian, *Acc. Chem. Res.*, 43 (2010) 1115.
18. C.-H. Kuo, Y. Tang, L.-Y. Chou, B. T. Sneed, C. N. Brodsky, Z. Zhao and C.-K. Tsung, *J. Am. Chem. Soc.*, 134 (2012) 14345.
19. D. Dang, P. Wu, C. He, Z. Xie and C. Duan, *J. Am. Chem. Soc.*, 132 (2010) 14321.
20. P. Horcajada, C. Serre, G. Maurin, N. A. Ramsahye, F. Balas, M. Vallet-Regi, M. Sebban, F. Taulelle and G. Ferey, *J. Am. Chem. Soc.*, 130 (2008) 6774.
21. T. J. Bandosz and C. Petit, *Adsorption*, 17 (2011) 5.
22. M. Ramezanzadeh, B. Ramezanzadeh, M. Mahdavian and G. Bahlakeh, *Carbon*, 161 (2020) 231.
23. L. Xiong, J. Liu, M. Yu and S. Li, *Corros. Sci.* 146 (2019) 70.
24. M. Xu, Y. Hu, W. Ding, F. Li, J. Lin, M. Wu, J. Wu, L.-P. Wen, B. Qiu, P.-F. Wei and P. Li, *Biomater.*, 258 (2020) 120308.
25. J. Cao, C. Guo, X. Guo and Z. Chen, *J. Mol. Liq.*, 311 (2020) 113277.
26. J. Yuan, R. Yuan, J. Wang, Q. Li, X. Xing, X. Liu and W. Hu, *Surf. Coat. Technol.*, 352 (2018) 74.
27. M. Miao, J. Wang and W. Hu, *Colloids Surf., A*, 543 (2018) 144.
28. C. S. Wu, Z. H. Xiong, C. Li and J. M. Zhang, *Rsc Adv.*, 5 (2015) 82127.
29. X. Liu, Y. Li, Y. Ban, Y. Peng, H. Jin, H. Bux, L. Xu, J. Caro and W. Yang, *Chem. Commun.*, 49 (2013) 9140.
30. L. Wu, D. Yang, G. Zhang, Z. Zhang, S. Zhang, A. Tang and F. Pan, *Appl. Surf. Sci.*, 431 (2018) 177.
31. R. Xiao, W. Wang, L. Pan, R. Zhu, Y. Yu, H. Li, H. Liu and S.-L. Wang, *J. Mater. Sci.*, 46 (2011) 2635.
32. N. Bagheri, A. Khataee, J. Hassanzadeh and L. Samaei, *Sens. Actuators, B*, 284 (2019) 220.
33. Q. Song, S. K. Nataraj, M. V. Roussanova, J. C. Tan, D. J. Hughes, W. Li, P. Bourgoïn, M. A. Alam, A. K. Cheetham, S. A. Al-Muhtaseb and E. Sivaniah, *Energy Environ. Sci.*, 5 (2012) 8359.
34. J. Ethiraj, F. Bonino, C. Lamberti and S. Bordiga, *Microporous Mesoporous Mater.*, 207 (2015) 90.
35. M. D. Destreri, J. Vogelsang and L. Fedrizzi, *Prog. Org. Coat.*, 37 (1999) 57.
36. S. Xie, J. Wang and W. Hu, *Int. J. Electrochem. Sci.*, 14 (2019) 6773.
37. Y. Liu, J. H. Pan, N. Wang, F. Steinbach, X. Liu and J. Caro, *Angew. Chemie. Int. Ed.*, 54 (2015) 3028.
38. M. Zhang, L. Ma, L. Wan, Y. Sun and Y. Liu, *Acs Appl. Mater. Interfaces*, 10 (2018) 2259.
39. L. Wu, Z. Zhang, F. Pan, A. Tang, G. Zhang and L. Liu, *Int. J. Electrochem. Sci.*, 12 (2017) 6352.